J|A|C|S
ARTICLES
Published on Web 05/06/2003

A Biofuel Cell with Electrochemically Switchable and Tunable Power Output

Eugenii Katz and Itamar Willner*

Contribution from the Institute of Chemistry, The Hebrew University of Jerusalem, Jerusalem 91904, Israel

Received January 2, 2003; E-mail: willnea@vms.huji.ac.il

Abstract: An electroswitchable and tunable biofuel cell based on the biocatalyzed oxidation of glucose is described. The anode consists of a Cu^{2+}-poly(acrylic acid) film on which the redox-relay pyrroloquinoline quinone (PQQ) and the flavin adenine dinucleotide (FAD) cofactor are covalently linked. Apo-glucose oxidase is reconstituted on the FAD sites to yield the glucose oxidase (GOx)-functionalized electrode. The cathode consists of a Cu^{2+}-poly(acrylic acid) film that provides the functional interface for the covalent linkage of cytochrome *c* (Cyt *c*) that is further linked to cytochrome oxidase (COx). Electrochemical reduction of the Cu^{2+}-poly(acrylic acid) films (applied potential −0.5 V vs SCE) associated with the anode and cathode yields the conductive Cu^0-poly(acrylic acid) matrixes that electrically contact the GOx-electrode and the COx/Cyt *c*-electrode, respectively. The short-circuit current and open-circuit voltage of the biofuel cell correspond to 105 μA (current density ca. 550 μA cm^{-2}) and 120 mV, respectively, and the maximum extracted power from the cell is 4.3 μW at an external loading resistance of 1 kΩ. The electrochemical oxidation of the polymer films associated with the electrodes (applied potential 0.5 V) yields the nonconductive Cu^{2+}-poly(acrylic acid) films that completely block the biofuel cell operation. By the cyclic electrochemical reduction and oxidation of the polymer films associated with the anode and cathode between the Cu^0-poly(acrylic acid) and Cu^{2+}-poly(acrylic acid) states, the biofuel cell performance is reversibly switched between "ON" and "OFF" states, respectively. The electrochemical reduction of the Cu^{2+}-polymer film to the Cu^0-polymer film is a slow process (ca. 1000 s) because the formation and aggregation of the Cu^0-clusters requires the migration of Cu^{2+} ions in the polymer film and their reduction at conductive sites. The slow reduction of the Cu^{2+}-polymer films allows for the controlling of the content of conductive domains in the films and the tuning of the output power of the biofuel cell. The electron-transfer resistances of the cathodic and anodic processes were characterized by impedance spectroscopy. Also, the overall resistances of the biofuel cell generated by the time-dependent electrochemical reduction process were followed by impedance spectroscopy and correlated with the internal resistances of the cell upon its operation.

Introduction

Electrical contacting of redox enzymes with electrode supports attracts substantial research efforts directed to the development of biosensors,[1,2] bioelectrocatalyzed chemical transformations,[3] and the development of biofuel cell elements.[4,5] Tethering of electroactive relays to redox proteins[6] or the immobilization of redox proteins in electroactive polymers[7] are common practices to electrically contact and activate the redox enzymes. Recently, we reported on the effective electrical contacting of redox enzymes on electrodes by their structural alignment on electrodes through the surface reconstitution of flavoenzymes or pyrroloquinoline quinone (PQQ)-dependent enzymes on a relay-FAD monolayer assembly[8] or redox polymer-PQQ thin film,[9] respectively. This concept was further generalized by tailoring integrated, electrically contacted, cofactor-dependent enzyme electrodes by the cross-linking of affinity complexes

(1) (a) Willner, I.; Katz, E. *Angew. Chem., Int. Ed.* **2000**, *39*, 1180−1218. (b) Willner, I.; Katz, E.; Willner, B. In *Biosensors and Their Applications*; Yang, V. C., Ngo, T. T., Eds.; Kluwer Academic Publishers: New York, 2000; Chapter 4, pp 47−98. (c) Willner, I.; Willner, B. *Trends Biotechnol.* **2001**, *19*, 222−230.
(2) (a) Bartlett, P. N.; Tebbutt, P.; Whitaker, R. C. *Prog. React. Kinet.* **1991**, *16*, 55−155. (b) Heller, A. *Acc. Chem. Res.* **1990**, *23*, 128−134. (c) Willner, I. *Science* **2002**, *298*, 2407−2408.
(3) Laane, C.; Pronk, W.; Fraseen, M.; Veeger, C. *Enzyme Microb. Technol.* **1984**, *6*, 165−168.
(4) (a) Palmore, G. T. R.; Bertschy, H.; Bergens, S. H.; Whitesides, G. M. *J. Electroanal. Chem.* **1998**, *443*, 155−161. (b) Tsujimura, S.; Tatsumi, H.; Ogawa, J.; Shimizu, S.; Kano, K.; Ikeda, T. *J. Electroanal. Chem.* **2001**, *496*, 69−75. (c) Chen, T.; Barton, S. C.; Binyamin, G.; Gao, Z. Q.; Zhang, Y. C.; Kim, H. H.; Heller, A. *J. Am. Chem. Soc.* **2001**, *123*, 8630−8631. (d) Mano, N.; Mao, F.; Heller, A. *J. Am. Chem. Soc.* **2002**, *124*, 12962−12963. (e) Katz, E.; Willner, I.; Kotlyar, A. B. *J. Electroanal. Chem.* **1999**, *479*, 64−68.
(5) Katz, E.; Shipway, A. N.; Willner, I. In *Handbook of Fuel Cells − Fundamentals, Technology, Applications*; Vielstich, W., Gasteiger, H., Lamm, A., Eds.; Wiley: Chichester, 2003; Vol. 1, Part 4, pp 355−381.
(6) (a) Schuhmann, W.; Ohara, T. J.; Schmidt, H.-L.; Heller, A. *J. Am. Chem. Soc.* **1991**, *113*, 1394−1397. (b) Willner, I.; Riklin, A.; Shoham, B.; Rivenzon, D.; Katz, E. *Adv. Mater.* **1993**, *5*, 912−915.
(7) (a) Heller, A. *J. Phys. Chem.* **1992**, *96*, 3579−3587. (b) Willner, I.; Willner, B. *React. Polym.* **1994**, *22*, 267−279. (c) Narvaez, A.; Suarez, G.; Popescu, I. C.; Katakis, I.; Dominguez, E. *Biosens. Bioelectron.* **2000**, *15*, 43−52.
(8) (a) Willner, I.; Heleg-Shabtai, V.; Blonder, R.; Katz, E.; Tao, G.; Bückmann, A. F.; Heller, A. *J. Am. Chem. Soc.* **1996**, *118*, 10321−10322. (b) Katz, E.; Riklin, A.; Heleg-Shabtai, V.; Willner, I.; Bückmann, A. F. *Anal. Chim. Acta* **1999**, *385*, 45−58. (c) Zayats, M.; Katz, E.; Willner, I. *J. Am. Chem. Soc.* **2002**, *124*, 2120−2121.
(9) Raitman, O. A.; Patolsky, F.; Katz, E.; Willner, I. *Chem. Commun.* **2002**, 1936−1937.

between NAD^+-dependent enzymes and an electrocatalyst-NAD^+ monolayer[10] or thin film[11] associated with electrodes. Efficient electron transfer between redox enzymes and conductive electrode supports as a result of structural alignment and optimal positioning of the electron mediators allowed the development of noncompartmentalized biofuel cells.[4e] Cross-reactions of the anolyte fuel and catholyte oxidizer with the opposite electrodes were prevented due to the high specificity of the bioelectrocatalytic reactions at the electrodes, and thus the use of a membrane separating the catholyte and anolyte solutions could be eliminated. This kind of biofuel cell was suggested as a self-powered biosensor for glucose or lactate, because the output voltage and current signals are dependent on the substrate concentration.[12] Also, enhanced electrical power output from biofeed cells was accomplished by the use of organic solvent/water two phase systems.[13]

The development of signal-controlled redox functionalities in molecular,[14] macromolecular,[15] and biomolecular[16] systems is directed to the design of information storage and processing systems, the development of new electronic materials, and the tailoring of molecular machinery systems. Photochemically controlled redox functions of molecular and supramolecular systems in solution were reported by the use of photoisomerizable components. Photoisomerization of molecular structures was reported to yield redox-activated states,[17] and light-induced translocations of redox units in supramolecular catenane or rotaxane assemblies by the photoisomerization of a light-sensitive molecular unit or photoinduced electron transfer were accomplished.[18,19] Similarly, pH-induced translocation of redox functionalities between distinct states in rotaxanes[20] represents a chemically controlled mechanical molecular function. The integration of redox-activated photoisomerizable molecular functionalities with electrodes in the form of monolayers was suggested as a general means for the electrochemical transduction of photonic information recorded by the photoactive interface.[21] Also, the photochemical translocation of a tethered redox-active cyclodextrin in a rotaxane assembly associated with an electrode was suggested as a light-driven molecular machine that electrochemically transduces its functional configuration.[22] Photoswitchable bioelectrocatalytic assemblies were suggested as a general method to develop optobioelectronic systems.[23] Tethering of photoisomerizable groups to redox enzymes,[24] reconstitution of apo-flavoenzymes with a photoisomerizable FAD-cofactor,[25] the use of photoisomerizable electron mediators,[26] and the organization of photoisomerizable monolayers as command interfaces that control the electrical contact of redox-proteins with the electrode[27] were reported as functional enzyme-based bioelectronic systems for the amperometric transduction of photonic signals. Recently, we reported on the development of magnetoswitchable bioelectrocatalytic systems in which external magnetic fields switch the bioelectrocatalytic functions of redox enzymes "ON" and "OFF".[28] Signal-controlled "smart" materials also include functional polymers. Functional polymers of controlled refractivity,[29] photochromic,[30] electrochromic,[31] and optoelectronic[32] functions were developed recently. The use of polymers with tunable refractive properties as optical modulators, optical filters, or electrooptic waveguide devices has been reported.[33] Similarly, polymers exhibiting photorefractive properties have been extensively used for optical storage of information.[34] Photochromic and electrochromic

(10) (a) Bardea, A.; Katz, E.; Bückmann, A. F.; Willner, I. *J. Am. Chem. Soc.* **1997**, *119*, 9114−9119. (b) Katz, E.; Heleg-Shabtai, V.; Bardea, A.; Willner, I.; Rau, H. K.; Haehnel, W. *Biosens. Bioelectron.* **1998**, *13*, 741−756.

(11) Raitman, O. A.; Katz, E.; Bückmann, A. F.; Willner, I. *J. Am. Chem. Soc.* **2002**, *124*, 6487−6496.

(12) Katz, E.; Bückmann, A. F.; Willner, I. *J. Am. Chem. Soc.* **2001**, *123*, 10752−10753.

(13) Katz, E.; Filanovsky, B.; Willner, I. *New J. Chem.* **1999**, *23*, 481−487.

(14) (a) Pease, A. R.; Jeppesen, J. O.; Stoddart, J. F.; Luo, Y.; Collier, C. P.; Heath, J. R. *Acc. Chem. Res.* **2001**, *34*, 433−444. (b) Collin, J.-P.; Dietrich-Buchecker, C.; Gavina, P.; Jimenez-Molero, M. C.; Sauvage, J.-P. *Acc. Chem. Res.* **2001**, *34*, 477−487. (c) Canevet, C.; Libman, J.; Shanzer, A. *Angew. Chem., Int. Ed. Engl.* **1996**, *35*, 2657−2660. (d) Goulle, V.; Harriman, A.; Lehn, J.-M. *J. Chem. Soc., Chem. Commun.* **1993**, 1034−1036. (e) Bethell, D.; Dougherty, G.; Cupertino, D. C. *J. Chem. Soc., Chem. Commun.* **1995**, 675−676.

(15) (a) Chegel, V.; Raitman, O.; Katz, E.; Gabai, R.; Willner, I. *Chem. Commun.* **2001**, 883−884. (b) Lahav, M.; Durkan, C.; Gabai, R.; Katz, E.; Willner, I.; Welland, M. E. *Angew. Chem., Int. Ed.* **2001**, *40*, 4095−4097. (c) Kepley, L. J.; Bard, A. J. *J. Electrochem. Soc.* **1995**, *142*, 4129−4138. (d) Suarez, M. F.; Compton, R. G. *J. Electroanal. Chem.* **1999**, *462*, 211−221.

(16) (a) Aizawa, M.; Haruyama, T.; Khan, G. F.; Kobatake, E.; Ikariyama, Y. *Biosens. Bioelectron.* **1994**, *9*, 601−610. (b) Bartlett, P. N.; Birkin, P. R.; Wang, J. H.; Palmisano, F.; De Benedetto, G. *Anal. Chem.* **1998**, *70*, 3685−3694. (c) Hamachi, I.; Hiraoka, T.; Yamada, Y.; Shinkai, S. *Chem. Lett.* **1998**, 537−538. (d) Pardo-Yissar, V.; Katz, E.; Willner, I.; Kotlyar, A. B. Sanders, C.; Lill, H. *Faraday Discuss.* **2000**, *116*, 119−134.

(17) (a) Takeshita, M.; Choi, C. N.; Irie, M. *Chem. Commun.* **1997**, 2265−2266. (b) Gilat, S. L.; Kawai, S. H.; Lehn, J.-M. *Chem.-Eur. J.* **1995**, *1*, 275−284. (c) Tsivgoulis, G. M.; Lehn, J.-M. *Chem.-Eur. J.* **1996**, *2*, 1399−1406. (d) Tsivgoulis, G. M.; Lehn, J.-M. *Adv. Mater.* **1997**, *9*, 39−42.

(18) (a) Ashton, P. R.; Ballardini, R.; Balzani, V.; Boyd, S. E.; Credi, A.; Gandolfi, M. T.; Gomez-Lopez, M.; Iqbal, S.; Philp, D.; Preece, J. A.; Prodi, L.; Ricketts, H. G.; Stoddart, J. F.; Tolley, M. S.; Venturi, M.; White, A. J. P.; Williams, D. J. *Chem.-Eur. J.* **1997**, *3*, 152−170. (b) Balzani, V.; Gomez-Lopez, M.; Stoddart, J. F. *Acc. Chem. Res.* **1998**, *31*, 405−414. (c) Murakami, H.; Kawabuchi, A.; Kotoo, K.; Kunitake, M.; Nakashima, N. *J. Am. Chem. Soc.* **1997**, *119*, 7605−7606.

(19) (a) Balzani, V.; Credi, A.; Raymo, F. M.; Stoddart, J. F. *Angew. Chem., Int. Ed.* **2000**, *39*, 3348−3391. (b) Balzani, V.; Credi, A.; Langford, S. J.; Raymo, F. M.; Stoddart, J. F.; Venturi, M. *J. Am. Chem. Soc.* **2000**, *122*, 3542−3543.

(20) (a) Bissell, R. A.; Cordova, E.; Kaifer, A. E.; Stoddart, J. F. *Nature* **1994**, *369*, 133−137. (b) Ballardini, R.; Balzani, V.; Credi, A.; Gandolfi, M. T.; Langford, S. J.; Menzer, S.; Prodi, L.; Stoddart, J. F.; Venturi, M.; Williams, D. J. *Angew. Chem., Int. Ed. Engl.* **1996**, *35*, 978−981.

(21) (a) Liu, Z.; Hashimoto, K.; Fujishima, A. *Nature* **1990**, *347*, 658−660. (b) Doron, A.; Katz, E.; Portnoy, M.; Willner, I. *Angew. Chem., Int. Ed. Engl.* **1996**, *35*, 1535−1537. (c) Doron, A.; Portnoy, M.; Lion-Dagan, M.; Katz, E.; Willner, I. *J. Am. Chem. Soc.* **1996**, *118*, 8937−8944. (d) Shipway, A. N.; Willner, I. *Acc. Chem. Res.* **2001**, *34*, 421−432. (e) Willner, I.; Willner, B. *J. Mater. Chem.* **1998**, *8*, 2543−2556. (f) Willner, I.; Willner, B. In *Molecular Switches*; Feringa, B. L., Ed.; Wiley−VCH: Weinheim, Germany, 2001; Chapter 6, pp 165−218.

(22) Willner, I.; Pardo-Yissar, V.; Katz, E.; Ranjit, K. T. *J. Electroanal. Chem.* **2001**, *497*, 172−177.

(23) (a) Willner, I.; Katz, E.; Willner, B.; Blonder, R.; Heleg-Shabtai, V.; Bückmann, A. F. *Biosens. Bioelectron.* **1997**, *12*, 337−356. (b) Willner, I.; Doron, A.; Katz, E. *J. Phys. Org. Chem.* **1998**, *11*, 546−560. (c) Katz, E.; Willner, B.; Willner, I. *Biosens. Bioelectron.* **1997**, *12*, 703−719. (d) Willner, I. *Acc. Chem. Res.* **1997**, *30*, 347−356.

(24) (a) Lion-Dagan, M.; Katz, E.; Willner, I. *J. Am. Chem. Soc.* **1994**, *116*, 7913−7914. (b) Willner, I.; Lion-Dagan, M.; Marx-Tibbon, S.; Katz, E. *J. Am. Chem. Soc.* **1995**, *117*, 6581−6592.

(25) (a) Willner, I.; Blonder, R.; Katz, E.; Stocker, A.; Bückmann, A. F. *J. Am. Chem. Soc.* **1996**, *118*, 5310−5311. (b) Blonder, R.; Katz, E.; Willner, I.; Wray, V.; Bückmann, A. F. *J. Am. Chem. Soc.* **1997**, *119*, 11747−11 757.

(26) Lion-Dagan, M.; Marx-Tibbon, S.; Katz, E.; Willner, I. *Angew. Chem., Int. Ed. Engl.* **1995**, *34*, 1604−1606.

(27) (a) Lion-Dagan, M.; Katz, E.; Willner, I. *J. Chem. Soc., Chem. Commun.* **1994**, 2741−2742. (b) Willner, I.; Doron, A.; Katz, E.; Levi, S.; Frank, A. J. *Langmuir* **1996**, *12*, 946−954.

(28) (a) Hirsch, R.; Katz, E.; Willner, I. *J. Am. Chem. Soc.* **2000**, *122*, 12053−12054. (b) Katz, E.; Willner, I. *Electrochem. Commun.* **2001**, *3*, 683−685. (c) Sheeney-Haj-Ichia, L.; Katz, E.; Wasserman, J.; Willner, I. *Chem. Commun.* **2002**, 158−159. (d) Katz, E.; Sheeney-Haj-Ichia, L.; Willner, I. *Chem.-Eur. J.* **2002**, *8*, 4138−4148.

(29) (a) Burland, D. M.; Miller, R. D.; Walsh, C. A. *Chem. Rev.* **1994**, *94*, 31−75. (b) Fouda, I. M. *J. Appl. Polym. Sci.* **2001**, *81*, 3349−3360.

(30) (a) Walheim, S.; Schaffer, E.; Mlynek, J.; Steiner, U. *Science* **1999**, *282*, 520−522. (b) Feng, W.; Zhang, T. R.; Liu, Y.; Wei, L.; Lu, R.; Li, T. J. Zhao, Y. Y.; Yao, J. N. *J. Mater. Res.* **2002**, *17*, 133−136.

(31) (a) Rosseinsky, D. R.; Mortimer, R. J. *Adv. Mater.* **2001**, *13*, 783−793. (b) Arman, S. *J. New Mater. Electrochem. Syst.* **2001**, *4*, 173−179. (c) Monk, P. M. S.; Mortimer, R. J.; Rosseinsky, D. R. *Electrochromism: Fundamentals and Applications*; VCH: Weinheim, 1995.

(32) (a) Grote, J. G.; Zetts, J. S.; Nelson, R. L.; Hopkins, F. K.; Dalton, L. R.; Zhang, C.; Steier, W. H. *Opt. Eng.* **2001**, *40*, 2464−2473. (b) Friend, R. H. *Pure Appl. Chem.* **2001**, *73*, 425−430. (c) Mitschke, U.; Baüerle, P. *J. Mater. Chem.* **2000**, *10*, 1471−1507.

polymers have been suggested as active materials for the development of smart windows,[35] and conductive polymers have been extensively employed as active components in electrically induced light-emitting devices (LEDs).[32] Recently, efforts have been directed toward the development of functional metal or semiconductor nanoparticle-polymer hybrid systems exhibiting tailored sensoric,[36] electronic,[37] and photoelectrochemical functions.[38] We recently reported on a hybrid copper-poly(acrylic acid) polymer that can be reversibly switched between an electroconductive state where aggregated Cu^0-nanoparticles provide metallic conductivity across the polymeric matrix and a nonconductive state when the polymer includes electrochemically oxidized Cu^{2+} ions.[39]

In the present paper, we wish to report on a novel configuration of a biofuel cell, in which the output power (voltage and current) can be reversibly switched between "ON" and "OFF" states and the magnitude of the voltage−current output can be precisely tuned by an electrochemical input signal. This is accomplished by the integration of the biocatalysts active in the biofuel cell with a copper-poly(acrylic acid) matrix. The assembly of the biocatalyst/copper-poly(acrylic acid) hybrid system with electrodes allows for the electrical control of the conductivity properties of the matrix, thus enabling the electroswitchable and tunable functions of the biofuel cell.

Experimental Section

Chemicals. Glucose oxidase (GOx, EC 1.1.3.4 from *Aspergillus niger*) was purchased from Sigma and used without further purification. Apo-glucose oxidase (apo-GOx) was prepared by a modification[8b] of the reported method.[40] Cytochrome oxidase (COx) was isolated from a Keilin−Hartree heart muscle and purified according to a published technique.[41] Yeast iso-2-cytochrome *c* (Cyt *c*) from *Saccharomyces cerevisiae* (Sigma) was purified by ion-exchange chromatography. N^6-(2-Aminoethyl)-flavin adenine dinucleotide was synthesized and purified as described before.[42] All other chemicals, including pyrroloquinoline quinone (PQQ), acrylic acid, methylene-bis-acrylamide, *N*-succinimidyl-3-maleimidopropionate, 4-(2-hydroxyethyl)piperazine-1 ethanesulfonic acid sodium salt (HEPES), tris(hydroxymethyl)aminomethane hydrochloride (TRIS), 1-ethyl-3-(3-dimethylaminopropyl)carbodiimide (EDC), glutaric dialdehyde, and β-D-(+)-glucose, were purchased from Sigma and Aldrich and used as supplied. Ultrapure water from Seralpur Pro 90 CN source was used in all of the experiments.

Modification of Electrodes. Glass supports (TF-1 glass, 20 × 20 mm) covered with a Cr thin sublayer (5 nm) and a polycrystalline Au layer (50 nm) supplied by Analytical-μSystem (Germany) were used as conductive supports. These electrodes were modified with a poly(acrylic acid) thin film using the electropolymerization technique.[43] The electropolymerization was performed in an aqueous solution composed of acrylic acid sodium salt, 2 M, methylene-bis-acrylamide, 0.04 M, and $ZnCl_2$, 0.2 M, pH = 7.0, upon application of five potential cycles (50 mV s^{-1}) between 0.1 and −1.5 V. A potential of 0.1 V was then applied for 1 min to dissolve electrochemically metallic zinc produced in the film upon the electrochemical polymerization. The polymer-modified electrode was reacted with 0.1 M HCl for 2 min to dissolve residual amounts of metallic zinc, and then the electrode was washed with water and ethanol to clean the modified surface from Zn^{2+} ions and the excess of monomers. The polymer-modified electrodes were soaked in 0.1 M $CuSO_4$ solution for 1 h to saturate the polyacrylic film with Cu^{2+} ions, and then the electrode surface was briefly washed with water. The modified electrodes were further reacted with a solution of polyethylenimine (MW 60 000) (5% v/v) in 0.1 M HEPES-buffer, pH = 7.2, in the presence of EDC, 1×10^{-2} M, for 1 h, and then washed with water. The polymer-modified electrode was incubated for 2 h in a 3 mM solution of PQQ (**1**) in 0.1 M HEPES-buffer, pH = 7.2, in the presence of 5×10^{-3} M EDC, yielding the PQQ-functionalized surface. The covalent coupling of N^6-(2-aminoethyl)-FAD (**2**) to the PQQ-modified electrode was performed by soaking the electrode in the 0.1 M HEPES-buffer solution (pH = 7.2) containing 5×10^{-4} M **2** and 5×10^{-3} M EDC for 2 h at room temperature. The PQQ-FAD dyad-functionalized electrode was reacted with 1 mg mL^{-1} apo-GOx in 0.1 M phosphate buffer, pH = 7.0, for 5 h at room temperature. The modified electrode was washed with water to yield the GOx-reconstituted electrodes for biocatalytic oxidation of glucose.[8] Another polymer-modified electrode was reacted with a 1×10^{-3} M solution of *N*-succinimidyl-3-maleimidopropionate (**3**) in 0.1 M HEPES-buffer, pH = 7.2, for 2 h, followed by rinsing with water. The maleimide-functionalized electrode was treated with Cyt *c* solution, 0.1 mM, in 0.1 M HEPES-buffer, pH 7.2, for 2 h, followed by rinsing with water. To produce the integrated Cyt *c*/COx bioelectrocatalytic electrode for O_2 reduction,[16d] the resulting Cyt *c*-modified electrode was interacted with cytochrome oxidase (COx), 0.5 mM, in TRIS-buffer, pH 8.0, for 2 h, washed briefly with water, and then treated with aqueous solution of glutaric dialdehyde, 10% v/v, for 30 min. The resulting modified electrode was washed with water.

Biofuel Cell and Electrochemical Measurements. Scheme 1A shows the biofuel cell configuration. The system consists of two enzyme-functionalized electrodes (ca. 0.19 cm^2 active area) separated by a rubber O-ring (ca. 2 mm thickness). The first electrode functionalized with the reconstituted GOx and the second electrode functionalized with Cyt *c*/COx assembly are acting as the anode and cathode, respectively. Two metallic needles (inlet and outlet) implanted into the rubber ring convert the unit into a flow cell (flow rate 1 mL min^{-1}). A peristaltic pump was applied to control the flow rate. Glucose solutions in 0.1 M TRIS-buffer, pH = 7.0, saturated with air were applied to power the biofuel cell. The needles were also used as a counter electrode and a quasi-reference electrode when electrochemical measurements were performed for each of the biomaterial-functionalized electrodes in the cell. The quasi-reference electrode was calibrated[44] according to the potential of dimethyl viologen, $E^\circ = -0.687$ V versus SCE, measured by cyclic voltammetry, and the potentials are reported versus SCE. Cyclic voltammetry and chronoamperometry experiments were performed using an electrochemical analyzer (EG&G model 283) linked to a computer (EG&G software 270/250). Impedance measurements were performed using an electrochemical analyzer composed of a

(33) (a) Steier, W. H.; Chen, A.; Lee, S. S.; Garner, S.; Zhang, H.; Chuyanov, V.; Dalton, L. R.; Wang, F.; Ren, A. S.; Zhang, C.; Todorova, G.; Harper, A.; Fetterman, H. R.; Chen, D. T.; Udupa, A.; Bhattachrya, D.; Tsap, B. *Chem. Phys.* **1999**, *245*, 487−506. (b) Donaldson, A. *J. Phys. D: Appl. Phys.* **1991**, *24*, 785−802.
(34) (a) Lucchetti, L.; Simoni, F. *Riv. Nuovo Cimento* **2000**, *23*, 1−28. (b) Moerner, W. E.; Silence, S. M. *Chem. Rev.* **1994**, *94*, 127−155.
(35) (a) Lampert, C. M. *Thin Solid Films* **1993**, *236*, 6−13. (b) *Large-Area Chromogenics: Materials and Devices for Transmittance Control*; Lampert, C. M., Grandqvist, C. G., Eds.; SPIE Proc., SPIE: Bellington, WA, 1988; Vol. IS4.
(36) (a) Godovsky, D. Y. *Adv. Polym. Sci.* **2000**, *153*, 163−205. (b) Bauer, G.; Pittner, F.; Schalkhammer, T. *Mikrochim. Acta* **1999**, *131*, 107−114. (c) Schalkhammer, T. *Monatsh. Chem.* **1998**, *129*, 1067−1092.
(37) (a) Sheeney-Haj-Ichia, L.; Sharabi, G.; Willner, I. *Adv. Funct. Mater.* **2002**, *12*, 27−32. (b) Selvan, S. T.; Hayakawa, T.; Nogami, M.; Möller, M. *J. Phys. Chem. B* **1999**, *103*, 7441−7448.
(38) (a) Pardo-Yissar, V.; Bourenko, T.; Wasserman, J.; Willner, I. *Adv. Mater.* **2002**, *14*, 670−673. (b) Khazraji, A. C.; Hotchandani, S.; Das, S.; Kamat, P. V. *J. Phys. Chem. B* **1999**, *103*, 4693−4700.
(39) Chegel, V. I.; Raitman, O. A.; Lioubashevski, O.; Shirshov, Y.; Katz, E.; Willner, I. *Adv. Mater.* **2002**, *14*, 1549−1553.
(40) Morris, D. L.; Buckler, R. T. In *Methods in Enzymology*; Langone, J. J., Van Vunakis, H., Eds.; Academic Press: Orlando, FL, 1983; Vol. 92, Part E, pp 413−417.
(41) Yonetani, T. *J. Biol. Chem.* **1961**, *236*, 1680.
(42) Bückmann, A. F.; Wray, V.; Stocker, A. In *Methods in Enzyhmology: Vitamins and Coenzymes*; McCormick, D. B., Ed.; Academic Press: Orlando, FL, 1997; Vol. 280, Part 1, p 360.
(43) Katz, E.; De Lacey, A. L.; Fernandez, V. M. *J. Electroanal. Chem.* **1993**, *358*, 261−272.
(44) Katz, E.; Schlereth, D. D.; Schmidt, H.-L. *J. Electroanal. Chem.* **1994**, *367*, 59−70.

Scheme 1. (A) The Biofuel Cell Configuration and (B) Scheme for Electrical Measurements[a]

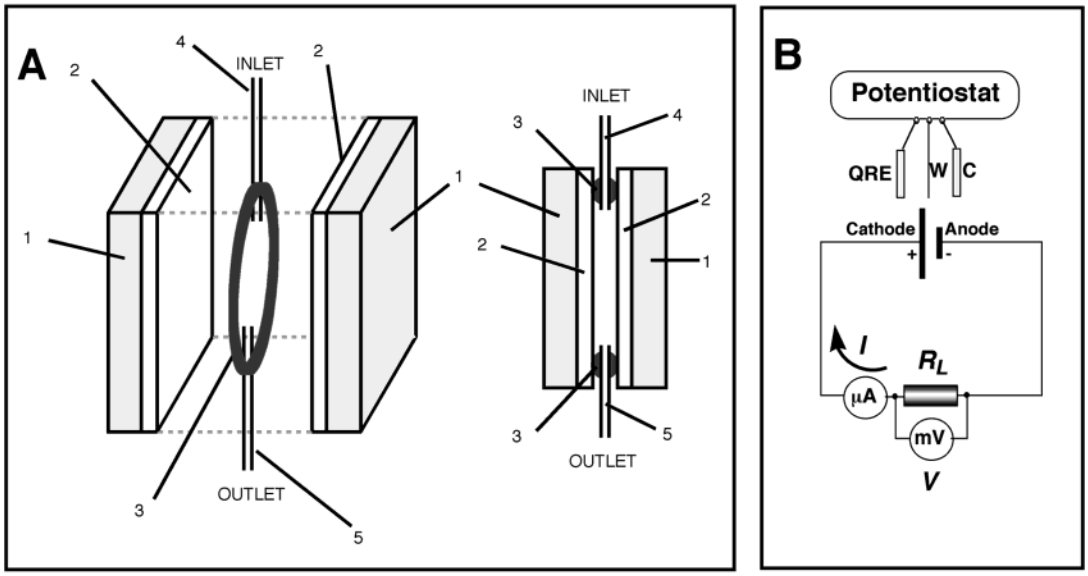

[a] (A) (1) Glass plate, 20 × 20 mm; (2) Au layer, 50 nm thickness; (3) O-ring, 16 mm internal diameter; (4) metallic needle, inlet; (5) metallic needle, outlet. (B) The biofuel cell output voltage and current are measured on the external variable load resistance, R_L, using an electrometer. The electrochemical measurements are performed on the cathode or anode of the cell connected to the working-electrode inlet of the potentiostat, W. Two metallic needles are used as a counter electrode, C, and as a quasi-reference electrode, QRE.

Scheme 2. Electrochemical Generation of the Polyacrylic Acid Film on a Au Electrode and the Assembly of the Integrated Cu^{2+}-Polymer Film Electrode

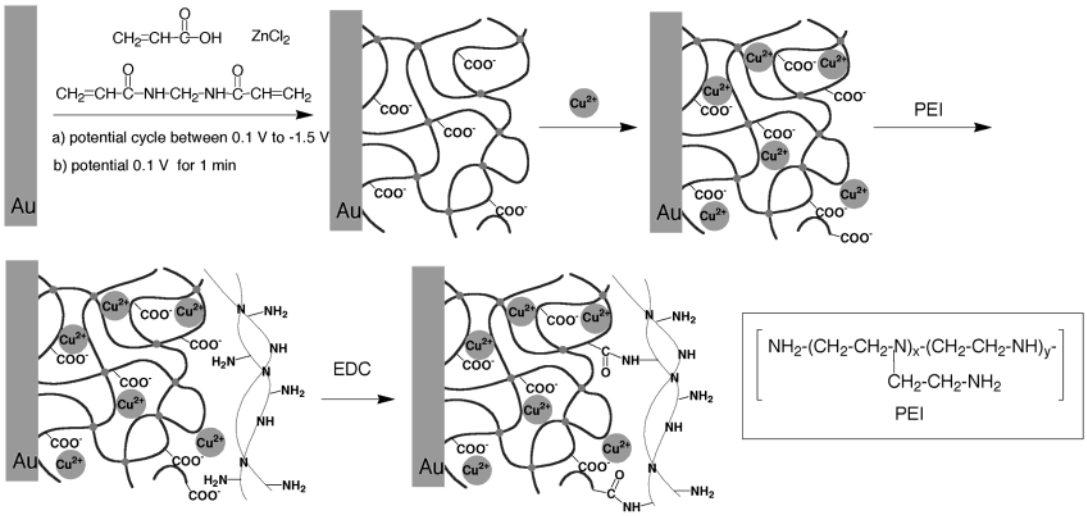

potentiostat/galvanostat (EG&G, model 283) and frequency response detector (EG&G model 1025) connected to a computer (EG&G software PowerSuite 2.11.1). The impedance measurements were performed in the frequency range of 100 mHz to 50 kHz between the cathode and anode of the biofuel cell (two-electrodes mode) and for each biocatalytic electrode using a counter electrode and a quasi-reference electrode (three-electrodes mode). The experimental impedance spectra were simulated using electronic equivalent circuits. For this purpose, commercial software (ZView version 2.1b, Scribner Associates, Inc.) was employed. Voltage and current produced by the biofuel cell were measured on a variable external resistance using an electrometer (Keithley 617), Scheme 1B.

Microgravimetric Quartz-Crystal Microbalance (QCM) Measurements. A QCM analyzer (Fluke 164T multifunction counter, 1.3 GHz, TCXO) and quartz crystals (AT-cut, 9 MHz, Seiko) sandwiched between two Au electrodes (area 0.2 ± 0.01 cm^2, roughness factor ca. 3.5) were employed for the microgravimetric analyses of the modified electrodes in air. The QCM crystals were calibrated by electropolymerization of aniline in 0.1 M H_2SO_4 and 0.5 M Na_2SO_4 electrolyte solution, followed by coulometric assay of the resulting polyaniline film and relating of the crystal frequency changes to the electrochemically derived polymer mass.

Results and Discussion

Acrylic acid as a monomer and methylene-bis-acrylamide as a cross-linker at a molar ratio of 50:1 were electropolymerized on gold electrodes (Au-covered glass slides) in the presence of $ZnCl_2$, 0.2 M, as catalyst to yield a poly(acrylic acid) thin film, Scheme 2.[43] The electropolymerization was performed by potential cycling (five cycles, 50 mV s^{-1}) between 0.1 and −1.5 V followed by application of 0.1 V for 1 min. The co-deposited metallic zinc produced at the negative potentials was electrochemically dissolved at the potential of 0.1 V. The residual traces of Zn^0 were dissolved in HCl, and the produced Zn^{2+} cations were washed off. The polymeric film was characterized by surface plasmon resonance, and the film thickness corresponded to ca. 280 nm.[39] The polymeric thin film was reacted

Scheme 3. Preparation and Operation of the Biocatalytic Anode[a]

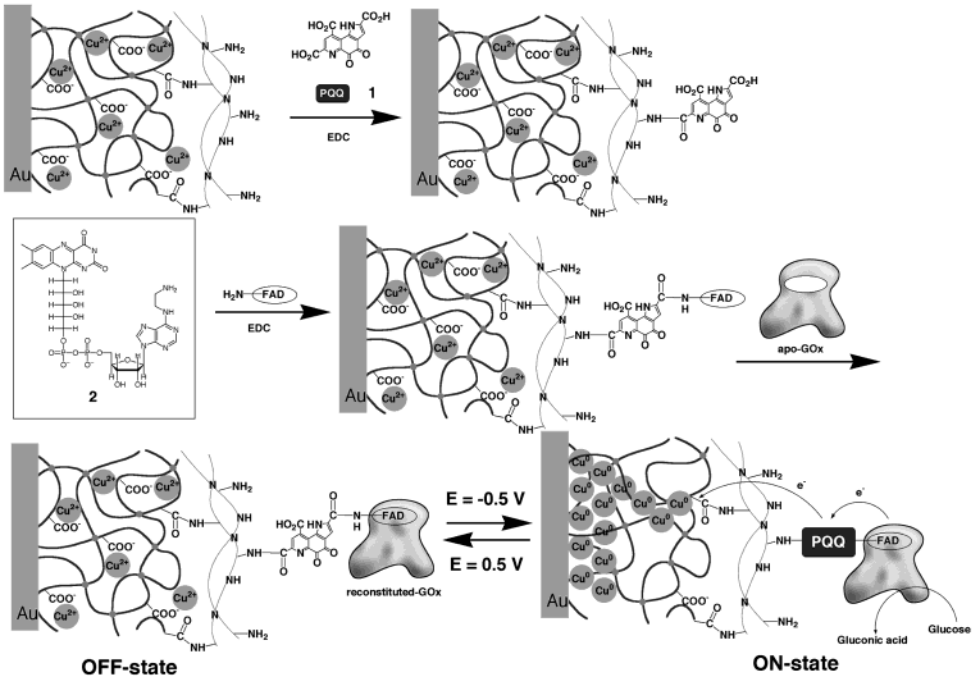

[a] Stepwise covalent binding of PQQ (**1**) and N^6-(2-aminoethyl)-flavin adenin dinucleotide (**2**) to the polymer-functionalized electrode followed by the reconstitution of apo-glucose oxidase, and reversible activation and deactivation of the biocatalytic anode by the electrochemical reduction of the Cu^{2+}-polymer film and the oxidation of the Cu^0-polymer film, respectively.

with 0.1 M $CuSO_4$ solution for 1 h to saturate the polymeric matrix with Cu^{2+} ions. The electrode surface was then reacted with polyethyleneimine in the presence of a carbodiimide coupling reagent (EDC). This resulted in the covalent attachment of the amine groups of polyethyleneimine to the carboxylic groups of the poly(acrylic acid) film, thus yielding a positively charged capping layer preserving Cu^{2+} ions inside the polymeric matrix and providing amine functional groups for further modification of the electrode. Microgravimetric quartz-crystal microbalance (QCM) measurements that follow the similar modification steps were performed on a QCM-electrode. These measurements reveal that the electrode surface loadings with the poly(acrylic acid) film, the Cu^{2+} ions, and the polyethyleneimine layer correspond to 3.1×10^{-5}, 4.5×10^{-6}, and 1.2×10^{-6} g cm^{-2}, respectively. The poly(acrylic acid)/Cu^{2+}/polyethyleneimine-functionalized electrode was reacted with pyrroloquinoline quinone (PQQ, **1**), and then with N^6-(2-aminoethyl)-FAD (**2**), Scheme 3. The PQQ-FAD dyad was then used to reconstitute apo-GOx with the FAD-cofactor and to provide mediated electron transfer via the PQQ-unit, thus yielding a biocatalytic interface for the glucose oxidation.[8] Quartz-crystal microbalance measurements for similar modification steps were performed on a QCM-electrode and reveal that the electrode loadings with PQQ, FAD, and GOx correspond to ca. 2×10^{-10}, 2×10^{-10}, and 3×10^{-12} mol cm^{-2}, respectively. These values are similar to a random densely packed monolayer coverages. A heterobifunctional reagent *N*-succinimidyl-3-maleimidopropionate was applied to attach covalently the iso-2-cytochrome *c* (Cyt *c*) to the polymer film, Scheme 4. The single-cysteine residue of the Cyt *c* was covalently linked to the maleimide functional group, providing alignment of the redox protein on the surface.[16d] Interaction of the Cyt *c*-functionalized surface with cytochrome oxidase (COx) resulted in a stable affinity complex between Cyt *c* and COx (association constant $K_a = 1.2 \times 10^7$ M^{-1}).[45] Cross-linking of the affinity complex with glutaric dialdehyde resulted in the integrated biocatalyst capable of reduction of O_2 to water, thus yielding a biocatalytic cathode.[16d] Quartz-crystal microbalance measurements for similar modification steps were performed on a QCM-electrode, and these reveal that the electrode loadings with Cyt *c* and COx are ca. 1×10^{-11} and 3×10^{-12} mol cm^{-2}, respectively. These surface densities correspond to a random densely packed Cyt *c* and COx monolayer configuration.[16d] The Cyt *c*/COx-functionalized electrode and the PQQ-FAD/GOx-functionalized electrode were assembled as a cathode and anode, respectively, in the flow biofuel cell configuration, Scheme 1A.

Figure 1A shows the cyclic voltammogram of the poly(acrylic acid)/Cu^{2+}/polyethyleneimine-functionalized electrode modified with the biocatalytic system (Cyt *c*/COx or PQQ-FAD/GOx) when the cell was loaded with a background electrolyte only (0.1 M TRIS-buffer, pH = 7.0, deaerated with Ar). The cyclic voltammogram was recorded using two metallic needles implanted into the cell as a counter electrode and a quasi-reference electrode. This cyclic voltammogram follows the known mechanism of the copper redox process.[46] Upon sweeping the potential from 0.7 to −0.6 V, a poorly resolved cathodic wave corresponding to the reduction of Cu^{2+} ions to Cu^+ ions is observed at $E_{pc1} = -0.05$ V, followed by the reduction wave of Cu^+ to Cu^0 at $E_{pc2} = -0.3$ V. Upon sweeping the potential back from −0.6 to 0.7 V, the reverse anodic peak is observed at $E_{pa1} = 0.18$ V, corresponding to the oxidation of Cu^0 to Cu^{2+}. The intermediate redox state Cu^+ is not observed because it undergoes disproportionation.[46] Coulometric analysis of the anodic redox wave ($E_{pa1} = 0.18$ V) recorded with a relatively fast potential scan rate (10 mV s^{-1}) yields the amount of Cu^{2+}/

(45) Kharitonov, A. B.; Alfonta, L.; Katz, E.; Willner, I. *J. Electroanal. Chem.* **2000**, *487*, 133−141.
(46) Gileadi, E.; Tsionsky, V. *J. Electrochem. Soc.* **2000**, *147*, 567−574.

Scheme 4. Preparation and Operation of the Biocatalytic Cathode[a]

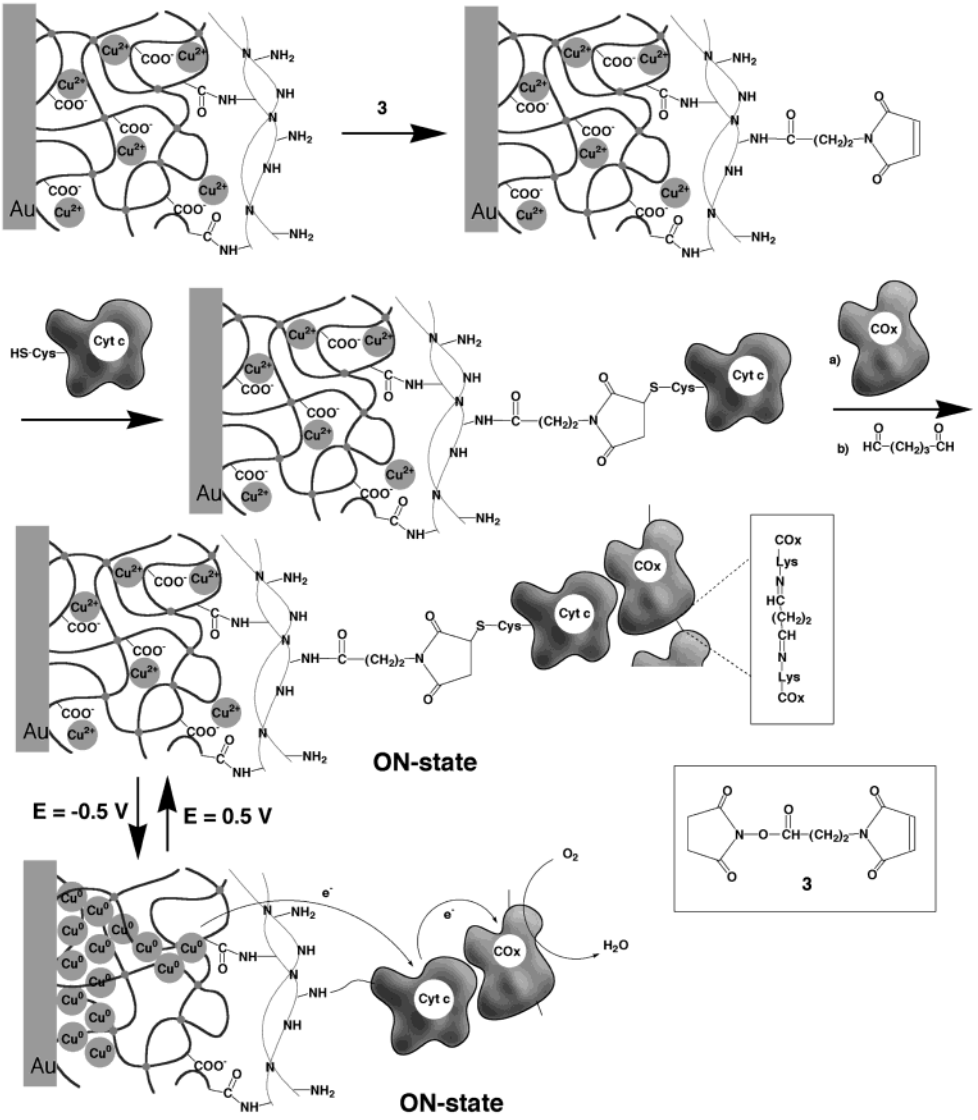

[a] Covalent attachment of iso-2-cytochrome *c* (Cyt *c*) to the polymer-functionalized electrode surface using *N*-succinimidyl-3-maleimidopropionate (**3**) as a heterobifunctional linker, followed by affinity binding of cytochrome oxidase (COx) and the crosslinking of the protein complex layer, and reversible activation and deactivation of the biocatalytic cathode by the electrochemical reduction of the Cu^{2+}-polymer film and the oxidation of the Cu^0-polymer film, respectively.

Cu^0 that participates in the redox process upon the potential scan (ca. 40 s at potentials lower than −0.2 V). The amount of redox-active copper found from the cyclic voltammogram is ca. 400 ng cm^{-2}, which is almost an order of magnitude smaller than the total amount of copper derived from the microgravimetric measurements. This discrepancy originates from slow charge propagation across the polymeric matrix; therefore, on the time scale of cyclic voltammetry, only the Cu^{2+} ions adjacent to the conductive support participate in the redox process. It should be noted that Cu^{2+} ions associated with the poly(acrylic acid) film capped with the polyethylenimine layer are not leaking from the membrane and the reproducible cyclic voltammogram could be observed in the absence of Cu^{2+} ions in the background solution upon application of many potential cycles.

To study the kinetics of the electrochemical reduction of Cu^{2+} ions across the polymeric matrix and the backward electrochemical oxidation of Cu^0 metallic particles, chronoamperometric measurements were performed. Figure 1B shows the cathodic current decay upon the potential step from 0.5 to −0.5 V. The kinetics of the reductive process, $\tau_{1/2} \approx 50$ s, corresponds to the formation of the conductive aggregates of Cu^0 particles across the polymeric matrix. The slow kinetics of this process is attributed to the fact that the Cu^{2+} ions have to migrate through the polymer film and reach the electrode surface to be reduced. Upon this reductive process, the conductive aggregates of Cu^0 nanoparticles are growing from the electrode surface and penetrating the polymer film. The amount of the reduced Cu^0 was derived by the integration of the cathodic current and corresponded to 4.4 μg cm^{-2} (6.9×10^{-8} mol cm^{-2}) after 1000 s of the reductive process. This surface loading is similar to that found by the quartz-crystal microbalance measurements. Taking into account the polymer film thickness of ca. 280 nm, as derived from the SPR measurements,[39] we calculated the concentration of the redox-active Cu^{2+}/Cu^0 in the film to be ca. 0.16 g cm^{-3} (2.5×10^{-3} mol cm^{-3}). The reductive process could be stopped at different time intervals (shown with arrows a−e in Figure 1B), providing various extents of the Cu^{2+} reduction and thus yielding different conductivities of the Cu^0-

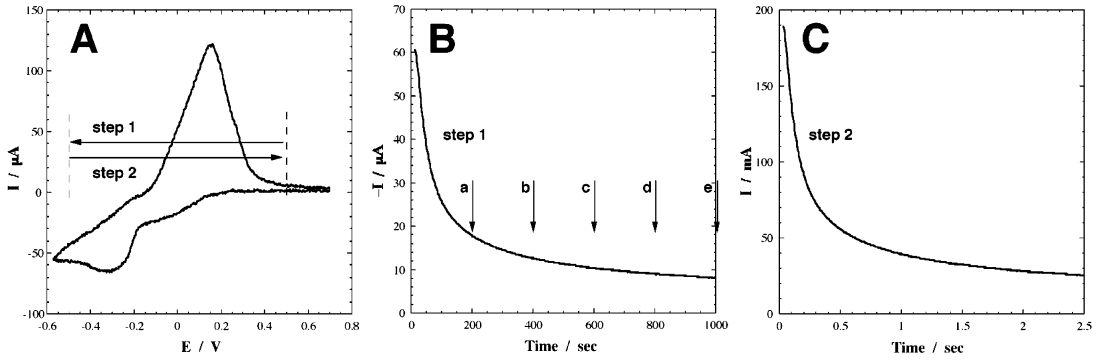

Figure 1. Electrochemical processes in the Cu^{2+}/Cu^0-poly(acrylic acid) hybrid thin film: (A) A cyclic voltammogram of the Cu^{2+}/Cu^0-poly(acrylic acid) hybrid film. Potential scan rate 10 mV s^{-1}. Arrows show the potential steps corresponding to the chronoamperometric measurements shown in parts B and C. (B) Cathodic current decay upon the application of a potential step from 0.5 to −0.5 V on the Cu^{2+}-polymer-functionalized electrode. Arrows a−e show the time interval applied for the electrochemical reduction of Cu^{2+} ions in the polymeric matrix. (C) Anodic current decay upon the application of a potential step from −0.5 to 0.5 V on the Cu^0-polymer-functionalized electrode after the potential of −0.5 V was applied on the electrode for 1000 s. The measurements were performed in the presence of 0.1 TRIS-buffer, pH = 7.0, in the cell under Ar.

polymeric matrix. Figure 1C shows the fast anodic current decay, $\tau_{1/2} \approx 0.2$ s, upon the potential step from −0.5 to 0.5 V after the potential of −0.5 V was applied to the electrode for 1000 s. The fast kinetics of this oxidative process (the oxidation of Cu^0 to Cu^{2+}) originates from the fact that the conductive assembly of the aggregated Cu^0 particles is already produced across the polymeric matrix prior to the potential step, thus providing the electrochemical contact of all of the Cu^0 species. The amount of the oxidized copper generated in the anodic process is derived by the integration of the anodic current, and it is similar to the amount of the reduced copper formed in the reductive process (ca. 4.4 μg cm^{-2}).

In the previous study,[39] we have demonstrated that the reduced Cu^0 species exist in the form of aggregated nanoparticles and the electrochemical transition between the Cu^0-polymeric matrix and the Cu^{2+}-polymeric matrix controls the electrical resistance of the film. While the Cu^{2+}-poly(acrylic acid) revealed very high resistance (transverse resistance between a Au 0.5 mm-diameter conductive tip and the electrode support, ca. 300 kΩ), the Cu^0-poly(acrylic acid) film exhibited lower resistance (ca. 2.2 kΩ). These properties of the Cu^{2+}/Cu^0-poly(acrylic acid) film suggest that the electrical contact between the electrode support and the redox biocatalyst associated with the film could be electrically switched and tuned by controlling the resistance of the polymer medium. To study the effect of the redox state of the Cu^{2+}/Cu^0-poly(acrylic acid) film on the biofuel cell output, the biocatalytic cathode and anode were preconditioned at the potentials of −0.5 V for 1000 s or at 0.5 V for 5 s to generate the reduced Cu^0 or oxidized Cu^{2+} in the film, respectively. The open circuit voltage and the short-circuit current (V_{oc} and I_{sc}) produced by the biofuel cell in these two states were measured in the presence of 80 mM glucose solution saturated with air, Scheme 1B. Figure 2 shows the reversible activation and deactivation of the biofuel cell upon the formation of the Cu^0 state and Cu^{2+} state, respectively. The biofuel cell short-circuit current is ca. 105 μA (current density ca. 550 μA cm^{-2}) in the active state (Cu^0-poly(acrylic acid)) and 0 μA in the nonactive state (Cu^{2+}-poly(acrylic acid)), Figure 2. The open-circuit voltage produced by the active state of the cell is ca. 120 and 0 mV in the Cu^{2+}-poly(acrylic acid) deactivated state of the cell, Figure 2. This is attributed to the fact that, in the reduced state, the Cu^0 nanoparticles generate the conductive aggregates, penetrating through the polymeric

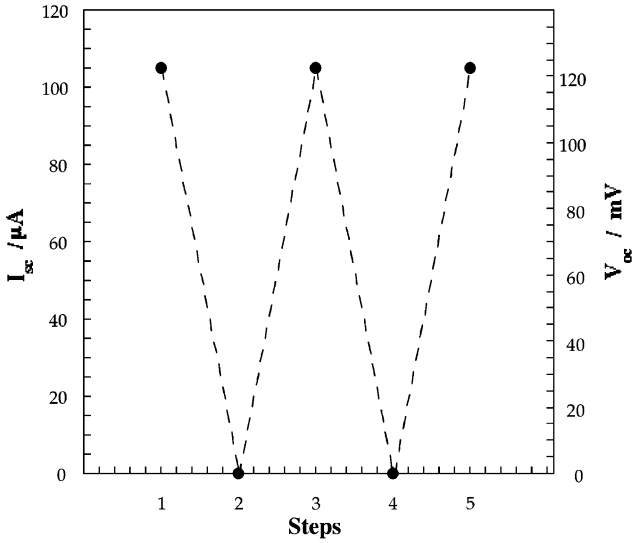

Figure 2. Reversible switching "ON" and "OFF" of the short-circuit current, I_{sc}, and the open-circuit voltage, V_{oc}, generated by the biofuel cell. The cell output is switched "ON" (steps 1, 3, and 5) by the application of the potential of −0.5 V to both biocatalytic electrodes for 1000 s and switched "OFF" (steps 2 and 4) by the application of a potential of 0.5 V to the two biocatalytic electrodes for 5 s. The measurements were performed in the presence of 80 mM glucose solution saturated with air.

matrix and providing electrical contacting of the biocatalyst with the electrode support. When the ionic state Cu^{2+} is electrochemically produced in the polymeric matrix, the biocatalysts are electrically disconnected from the electrode support, and the biocatalytic process cannot yield the voltage and current formation across the cell. Thus, the complete switching "ON" and "OFF" was achieved for the biofuel cell upon conditioning the biocatalytic electrodes at the reductive potential of −0.5 V for 1000 s and at the oxidative potential of 0.5 V for 5 s, respectively, Schemes 3 and 4. It should be noted that both electrodes (the cathode and anode) should be activated by the application of the reductive potential of −0.5 V to activate the entire biofuel cell; however, application of the oxidative potential of 0.5 V on any of the biocatalytic electrodes results in the biofuel cell deactivation. The open-circuit voltage produced by the active state of the cell, V_{oc} = 120 mV, almost corresponds to the maximum theoretical value[5] determined by the difference of the redox potentials of PQQ and cytochrome *c* (E_{PQQ}° =

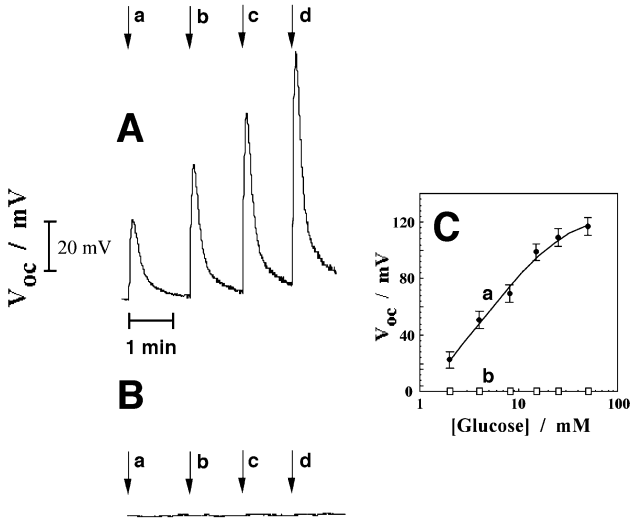

Figure 3. Open-circuit voltage (V_{oc}) at a variable concentration of glucose injected into the biofuel cell device: (A) After the anode and cathode of the biofuel cell were activated by the application of the potential corresponding to −0.5 V for 1000 s. (B) After the anode and cathode of the biofuel cell were deactivated by the application of the potential of 0.5 V for 5 s. Arrows show the injection of glucose with the concentrations of: (a) 2 mM, (b) 3 mM, (c) 8 mM, (d) 40 mM. (C) Calibration plots of the glucose sensing when the biofuel cell is activated (a) and deactivated (b). In all measurements, the glucose solution was equilibrated with air. The glucose samples of variable concentration (50 μL) in 0.1 M TRIS-buffer, pH = 7.0, were injected into the flow stream (flow rate of 1 mL min^{-1}).

−0.125 V[44] and $E_{Cyt}^{\circ} = 0.03$ V[16d]), which mediate the electron-transfer processes between the biocatalyst units and the electrodes.

In our previous study,[13] we have shown that a noncompartmentalized biofuel cell based on the reconstituted glucose oxidase and the integrated cytochrome *c*/cytochrome oxidase can function as a self-powered biosensor for glucose, producing an output voltage that is dependent on the glucose concentration. The present biofuel cell also shows that the output voltage signal is controlled by the glucose concentrations in the system, when the biocatalytic electrodes are activated to the conductive state by their preconditioning at the potential of −0.5 V for 1000 s, Figure 3A. Injection of air-saturated solutions with the different glucose concentrations resulted in the variable voltage signals generated by the cell, thus allowing the glucose sensing. The voltage output increases as the concentration of glucose is elevated. However, when any of the biocatalytic electrodes (the anode or cathode) are deactivated by the application of the oxidative potential of 0.5 V for 5 s, the cell voltage output is blocked to any glucose concentration, and thus the glucose biosensor is switched "OFF", Figure 3B. Figure 3C shows the calibration plots for the self-powered glucose biosensor when it is in the "ON" state, curve a, and in the "OFF" state, curve b.

The slow kinetics characteristic to the reduction of the matrix and its transformation to the conductive medium allow us to terminate the process at different time intervals and to achieve variable degrees of conductivity of the film. The controlled conductivity of the film could then be used to tune the voltage−current output of the biofuel cell. The reductive process was terminated after 200, 400, 600, 800, and 1000 s, resulting in different voltage−current outputs of the cell. Figure 4A shows the voltage−current density curves of the biofuel cell in the presence of 80 mM glucose solution saturated with air. The voltage−current density curves were measured at variable loading resistances (loading function)[47] after the application of the reduction process on the electrodes for different time intervals. It can be seen that the voltage−current output of the biofuel cell becomes higher when the reductive process applied on the Cu^{2+}/poly(acrylic acid) film is longer. The reductive process performed for 1000 s resulted in the highest output values. Figure 4B shows the electrical power density produced by the biofuel cell at variable resistances after application of the reductive potential on the biocatalytic electrodes for the different time intervals. It can be seen that the power output from the biofuel cell is smaller as the time interval for the reduction of the Cu^{2+}-polymer film to the Cu^0-polymer film is shorter. Also, we observe that the output power is less dependent on the value of the external resistances as the time interval for the generation of the Cu^0- polymer film is shorter. As the maximum value of the power output should occur at the external resistance load that is equal to the internal cell resistance,[47] the results imply that at shorter time intervals for the generation of the Cu^0-polymer film the cell resistance is higher. This conclusion can be explained by the fact that at shorter time intervals for generating the Cu^0-polymer a substantial amount of the polymer film exists in a nonconductive state with high resistance and the biocatalysts in these polymer domains are inactive. This conclusion will be further supported by impedance measurements, vide infra. When the reductive process that yields the Cu^0 state is longer, the conductivity of the hybrid film is increased, and the electrical contacting of the biocatalysts and the electrodes is improved. This results in the decrease of the electron-transfer resistance of the biocatalytic electrodes and yields smaller internal resistance of the biofuel cell. It should be noted that the internal resistance of the biofuel cell represents mainly the electron-transfer resistance of the biocatalytic electrodes.[47] As the time interval for the reduction of the Cu^{2+}-polymer film is shorter, the content of electrically contacted biocatalyst with the electrode is lower, and thus the average electron-transfer resistance is higher. The smaller internal resistance of the cell allows the higher voltage and current outputs, Figure 4A, but results in the sharp dependence of the produced power on the loading resistance values, Figure 4B. Thus, variation of the reductive time intervals applied to the biocatalytic electrodes allows the tuning of the output functions of the biofuel cell due to the change of the internal resistance of the cell.

The mechanism suggested for the electrochemical switching of the biofuel cell between "ON" and "OFF" states was further supported by Faradaic impedance measurements.[48] Impedance spectroscopy provides an effective method to probe the electron-transfer resistances at electrodes. A typical Faradaic impedance spectrum presented as a Nyquist plot (Z_{im} vs Z_{re}) consists of a semicircle domain at high frequencies. The diameter of the semicircle corresponds to the interfacial electron-transfer resistance.[48] Figure 5 shows the impedance spectra measured between the biocatalytic electrodes (two-electrodes mode)[49] in the presence of 80 mM glucose solution saturated with air.

(47) Bockris, J. O'M.; Srinivasan, S. *Fuel Cells: Their Electrochemistry;* McGraw-Hill Book Co.: New York, 1969.
(48) (a) Bard, A. J.; Faulkner, L. R. *Electrochemical Methods: Fundamentals and Applications*; Wiley: New York, 1980. (b) Stoynov, Z. B.; Grafov, B. M.; Savova-Stoynova, B. S.; Elkin, V. V. *Electrochemical Impedance*; Nauka: Moscow, 1991. (c) Katz, E.; Willner, I. *Electroanalysis* **2003**, in press.

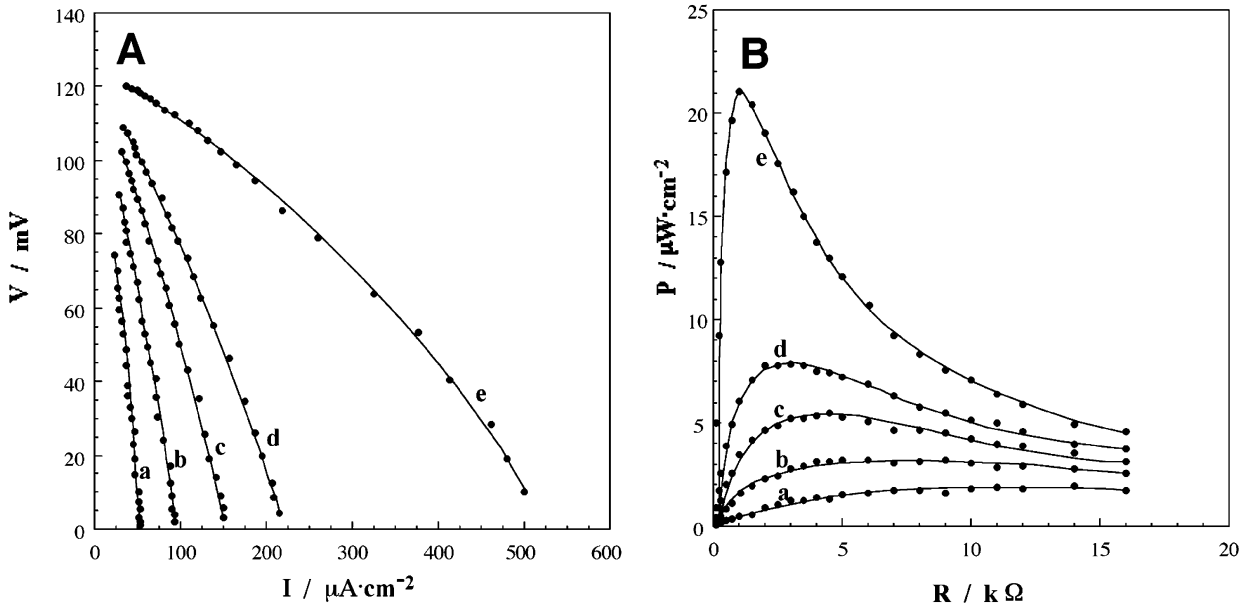

Figure 4. (A) Current density−voltage behavior of the biofuel cell at different external load resistances. (B) Electrical power density extracted from the biofuel cell at different external load resistances. Curves a−e show the biofuel cell output functions after the reductive potential of −0.5 V was applied to the biocatalytic electrodes for different time intervals: (a) 200 s, (b) 400 s, (c) 600 s, (d) 800 s, and (e) 1000 s. The measurements were performed in the presence of 80 mM glucose solution saturated with air. The electrode areas were ca. 0.19 cm^2.

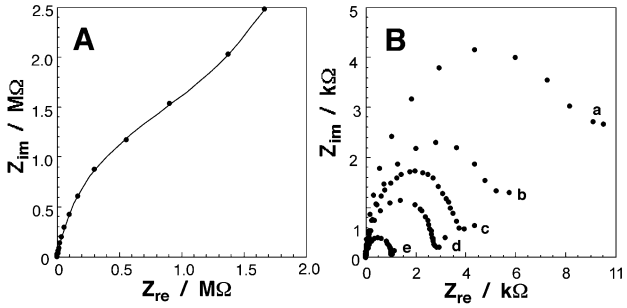

Figure 5. Nyquist plots (Z_{im} vs Z_{re}) corresponding to the impedance spectra of the biofuel cell measured between the cathode and anode (two-electrodes mode) in the presence of 80 mM glucose solution saturated with air. (A) The biofuel cell is in the "OFF" state after the potential of 0.5 V was applied on the two biocatalytic electrodes for 5 s. (B) The biofuel cell is in the "ON" state after the potential of −0.5 V was applied on both biocatalytic electrodes for different time intervals: (a) 200 s, (b) 400 s, (c) 600 s, (d) 800 s, and (e) 1000 s.

Figure 5A shows the impedance spectrum of the cell after the biocatalytic electrodes were deactivated by the application of the oxidative potential of 0.5 V for 5 s. The low frequency (0.1−1 Hz) impedance domain shows very high impedance values (Z_{im} and Z_{re}) of ca. 1−2 MΩ . Under this condition, the biofuel cell does not generate any measurable voltage−current output. Figure 5B, curve e, shows the impedance spectrum of the cell after the biocatalytic electrodes were fully activated by the application of the reductive potential of −0.5 V for 1000 s. The diameter of the semicircle domain of the spectrum corresponds to the overall electron-transfer resistance of the biofuel cell, $R_{et} \approx 1$ kΩ . This value is similar to the value of the external loading resistance that provides the maximum power produced by the fully activated biofuel cell, Figure 4B, curve e. It should be noted that the maximum power output is achieved at the external loading resistance equal to the internal resistance of the battery (or fuel cell).[47] Thus, the electron-transfer resistance, R_{et}, derived from the impedance spectrum, Figure 5B, curve e, corresponds to the internal resistance of the biofuel cell that operates in the fully activated state of the Cu^0-poly-(acrylic acid)-functionalized electrodes. Figure 5, curves a−e, shows the Faradaic impedance spectra measured between the biocatalytic electrodes (two-electrodes mode) upon operation of the biofuel cell after the reductive potential of −0.5 V was applied to the electrodes for different time intervals. Curve e shows the impedance spectrum corresponding to the fully activated biofuel cell after application of the reductive potential of −0.5 V for 1000 s. Curves a−d show the impedance spectra corresponding to the partially activated biofuel cell after the reductive potential of −0.5 V was applied on the electrodes for 200, 400, 600, and 800 s, respectively. These spectra, curves a−d, correspond to the intermediate tunable states of the biofuel cell that operates between the fully deactivated state, Figure 5A, and the fully activated state, Figure 5B, curve e. The electron-transfer resistances derived from the spectra, Figure 5B, curves a−d, correspond to ca. 12, 6, 4, and 2.7 kΩ , respectively. Thus, the electron-transfer resistances of the biofuel cell in its different degrees of electrochemical activation represent the internal resistances of the respective activated cells under operating conditions.

The overall electron-transfer resistance of the fuel cell derived from the impedance spectrum measured between the cathode and anode (two-electrodes mode) is composed of the partial electron-transfer resistances of the cathode and the anode that were measured separately (three-electrodes mode).[50] The later measurements were performed for each of the biocatalytic electrodes using a counter electrode and a quasi-reference

(49) (a) Rodrigues, S.; Munichandaraiah, N.; Shukla, A. K. *J. Power Sources* **2000**, *87*, 12−20. (b) Karden, E.; Buller, S.; De Doncker, R. W. *Electrochim. Acta* **2002**, *47*, 2347−2356. (c) Karden, E.; Buller, S.; De Doncker, R. W. *J. Power Sources* **2000**, *85*, 72−78. (d) Andersson, H.; Petersson, I.; Ahlberg, E. *J. Appl. Electrochem.* **2001**, *31*, 1−11. (e) Cheng, S.; Zhang, J.; Zhao, M.; Cao, C. *J. Alloys Compd.* **1999**, *293*−*295*, 814−820.

(50) Song, J. Y.; Lee, H. H.; Wan, C. C. *J. Power Sources* **2002**, *111*, 255−267.

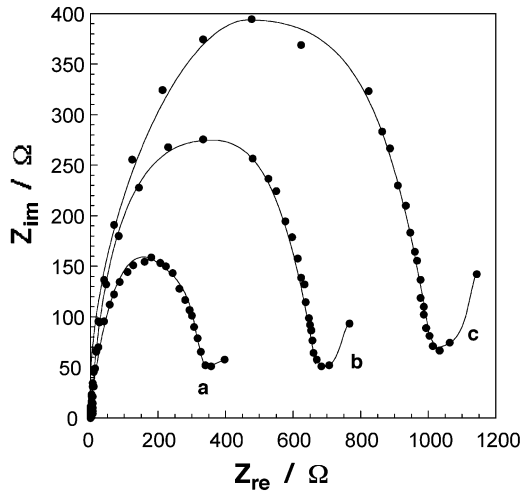

Figure 6. Nyquist plots (Z_{im} vs Z_{re}) corresponding to the impedance spectra of: (a) the GOx-functionalized anode (three-electrodes mode), (b) the Cyt *c*/COx-functionalized cathode (three-electrodes mode), (c) the whole biofuel cell (two-electrodes mode). The measurements were performed in the presence of 80 mM glucose solution saturated with air, and after the biocatalytic electrodes were activated by the application of the potential of −0.5 V for 1000 s.

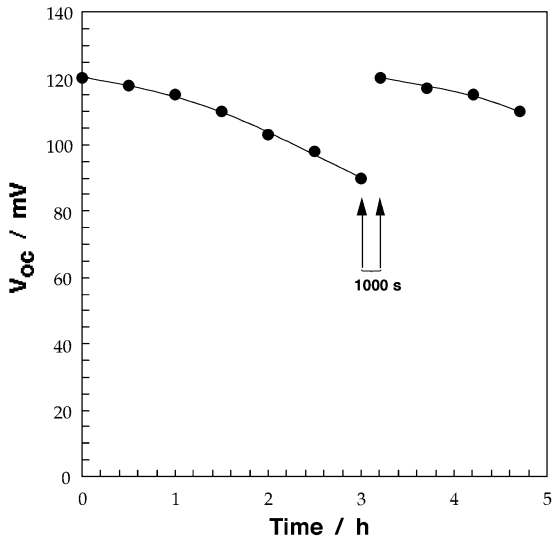

Figure 7. Time-dependent open-circuit voltage, V_{oc}, generated by the biofuel cell in the presence of 80 mM glucose solution saturated with air. Arrows show the time interval when the cell was reactivated by the application of the potential of −0.5 V on the biocatalytic cathode for 1000 s.

electrode in the cell, Scheme 1B. Figure 6, curve a, shows the impedance spectrum of the GOx-functionalized anode in the presence of 80 mM glucose solution saturated with air after the electrode was preconditioned at the potential of −0.5 V for 1000 s. The electron-transfer resistance of 340 Ω is derived from this spectrum. Figure 6, curve b, shows the impedance spectrum of the Cyt *c*/COx-functionalized cathode in the presence of 80 mM glucose solution saturated with air after the electrode was preconditioned at the potential of −0.5 V for 1000 s. The electron-transfer resistance of 660 Ω is derived from this spectrum. The overall electron-transfer resistance of the biofuel cell measured between the anode and cathode (two-electrodes mode) is ca. 1000 Ω, and this value fits nicely the sum of the electron-transfer resistances of the cathode and anode measured separately, as predicted theoretically.[50] It should be noted that the electron-transfer resistances of the anodic and the cathodic processes as well as the overall electron-transfer resistance of the cell (curves a, b, and c, respectively) represent the electrochemical kinetics of these processes rather than the ohmic resistances of the Cu^0-poly(acrylic acid) films on the electrodes. Particularly, the difference of the electron-transfer resistances of the anodic and cathodic processes originates from the difference in the respective electrochemical kinetics. From these impedance measurements, one can conclude that the main contribution to the biofuel cell electron-transfer resistance originates from the electron-transfer resistance of the Cyt *c*/COx-functionalized cathode. Thus, the cathodic biocatalytic process represents the limiting step in the whole biofuel cell operation. The same conclusion was previously extracted from the kinetic measurements performed for the similar biocatalytic systems.[12]

The last issue that should be addressed in this study is the biofuel cell operational stability. Because a positive potential is generated on the biocatalytic cathode upon the cell operation, the conductive Cu^0-state could be degraded due to the copper oxidation, thus resulting in the biofuel cell gradual deactivation. Figure 7 shows the biofuel cell voltage output (V_{oc}) measured upon continuous cell operation in the presence of 80 mM glucose solution saturated with air pumped through the cell with the flow rate of 1 mL min^{-1}. The open-circuit voltage slowly decreases from 120 to 90 mV after 3 h of continuous operation. After that, the reductive potential of −0.5 V was applied for 1000 s to the biocatalytic cathode, resulting in full reactivation of the cell and restoring the original V_{oc} = 120 mV. One can conclude from this result that the gradual decrease of the cell output originates from the partial oxidation of the conductive Cu^0-polymeric matrix associated with the cathode, rather than from the degradation of the enzyme-biocatalytic systems. The biofuel cell performance could be maintained with no efficiency loss for at least 48 h by the sequential reactivation steps that involve the application of the reductive potential on the cathode every 3 h (16 reactivation steps).

Conclusions

A noncompartmentalized biofuel cell composed of a biocatalytic anode based on the reconstituted glucose oxidase and a biocatalytic cathode based on the integrated cytochrome *c*/cytochrome oxidase was studied. The biocatalytic systems were assembled on the hybrid Cu^{2+}/Cu^0-poly(acrylic acid) matrix associated with the anode and cathode. The Cu^{2+}-poly(acrylic acid) associated with the electrodes is electrochemically reduced to the Cu^0-polymer conductive state, while the oxidation of the Cu^0-poly(acrylic acid) yields the nonconductive Cu^{2+}-polymer state. In the conductive state of the Cu^0-polymer film, the linked biocatalytic systems are electrically contacted with the electrode support, thus allowing the biofuel cell operation. In the nonconductive state of the Cu^{2+}-polymer film, the enzyme systems lack electrical contact with the electrodes, thus resulting in the high electron-transfer resistances switching "OFF" the biofuel cell performance. The cyclic electrochemical switching "ON" and "OFF" of the biofuel cell was achieved by the reversible application of the reductive potential of −0.5 V on the biocatalytic electrodes for 1000 s, and by the application of the oxidative potential of 0.5 V on the electrodes for 5 s, respectively. This switching process allowed the reversible activation and deactivation of the biofuel cell operation as a power source or as a self-powered glucose sensor.

Application of the reductive potential of −0.5 V for shorter time intervals (<1000 s) results in the partial reduction of the hybrid polymer film to the Cu^0-poly(acrylic acid) state, thus allowing tuning of the biofuel cell output. The impedance measurements performed on the biofuel cell allowed us to correlate the electron-transfer resistance values at the electrodes with the voltage−current and power−resistance functions of the biofuel cell. The impedance measurements performed for the individual biocatalytic electrodes (three-electrodes mode) and for the whole biofuel cell (two-electrodes mode) demonstrate that the overall electron-transfer resistance is composed of the electron-transfer resistances of the cathode and anode and that the electron-transfer resistance of the cathode is the main contributor to the cell resistance. Thus, the biocatalytic process of the Cyt *c*/COx-system is the limiting step in the biocatalytic cell operation. Long-term operation (>48 h) of the biofuel cell could be maintained by sequential short-time application of the reductive potential of −0.5 V on the cathode to restore the conductivity of the Cu^0-polymer matrix.

The present system represents the first example of an electrochemically switchable and tunable biofuel cell. A possible future application of such biofuel cell involves, for example, an implantable device that uses physiological fluids, for example, blood, for the generation of electrical power that activates machinery units such as pacemakers or insulin pumps. The switchable biofuel cell will enable the generation of the electrical output only upon the demand of the power consuming units, and the tunable operation of the cell will allow one to adjust the electrical power output as needed. It should be noted that the internally switchable and tunable activities of the biofuel cell have an important advantage over the positioning of an external tunable load to control the cell operation. While an external load would generate a voltage on the electrodes that might oxidize/reduce physiological ingredients, thereby generating harmful side effects, the electrochemical switching of the biofuel cell lacks these disadvantages.

Acknowledgment. This study is supported by the German-Israeli Binational Program (DIP).

JA034008V